Explicit Complex Solutions to the Fresnel Coefficients

Patrizia Savi, Yuekun Pei, and Albert J. Milani

Abstract – Global navigation satellite system reflectometry is a microwave remote sensing technique which can be used to derive information about the composition or properties of ground surfaces. The received power of the GPS signals reflected by the ground is proportional to the magnitude of the reflection Fresnel coefficients. In particular, it depends on the incidence angle θ and on the ground's permittivity ε. The knowledge of ε is important for determining various conditions and characteristics of the surface (for example, soil moisture, salinity, freeze-thaw transitions). The value of ε can be found from the Fresnel reflection coefficients, for a given incidence angle θ. For dispersive media, ε is a complex quantity; we present explicit formulas which express both $\Re(\varepsilon)$ and $\Im(\varepsilon)$ as a function of the incident angle θ and the magnitude of the linearly polarized Fresnel reflection coefficients.

1. Introduction

Global navigation satellite system reflectometry (GNSS-R) is a technique for sensing the Earth's surface, whereby GNSS signals reflected off the ground are detected and processed to monitor its properties remotely [1]. Important applications of this technique include ocean observation [2], ice [3, 4] and land remote sensing [5–7], altimetry [8, 9], and climate modeling and weather prediction [10]. This technique uses a passive bistatic radar configuration, which requires no transmitters except GNSS satellites, thus enabling the system to be light and compact [11, 12]. The signal-to-noise-ratio (SNR) data recorded by GNSS receivers are related to the direct signals and those reflected by the ground; if the surface is assumed flat, and the receiving antenna is either vertically or horizontally polarized, the SNR is related to the Fresnel reflection coefficients for vertical and horizontal polarization, which are functions of the relative permittivity ε of the soil and of the incident angle θ. The knowledge of ε allows for the determination of the soil moisture, by means of several well-established models (see for example the semiempirical models of [13, 14]), which may be useful for monitoring a field of known characteristics in terms of sand, clay percentage, and so on. In more general cases—that is, for non-flat surfaces—more powerful techniques of inverse scattering should be used [15]. We are interested in solving the inverse problem, consisting of finding the value of ε from the available measured values of the Fresnel reflection coefficients, for a given incidence angle θ. For nondispersive media, such as dry soil, the imaginary part of ε can be neglected, and it is sufficient to determine its real part. In contrast, for dispersive media, such as moist soils or sea salinity, it is important to also determine the imaginary part of ε. To our knowledge, the real and imaginary parts of ε have been determined only with empirical models, or by solving the Fresnel coefficient equations numerically.

In this work, we present formulas which express both $\Re(\varepsilon)$ and $\Im(\varepsilon)$ as explicit functions of the incident angle θ and the magnitude of the linearly polarized Fresnel reflection coefficients defined at the boundary between two dielectric media. Section 2 contains a detailed formulation of the problem; in section 3 the explicit formulas for the evaluation of ε are provided; in section 4 some tests confirming the validity of these formulas are indicated; and finally, section 5 contains some conclusions.

2. Statement of the Problem

A standard GNSS-R system collects the direct signals coming from the satellites (right-hand circularly polarized) with an up-looking antenna and the signals after reflection from the ground (left-hand circularly polarized) with a down-looking antenna [13] (see Figure 1). Even if most systems work with circular polarized antennas, measurements can also be carried out with linear polarized antennas (vertical and horizontal). The total electromagnetic field received by the down-looking antenna scattered by the Earth's surface is determined by coherent and incoherent components [16]. If the surface is approximately smooth, the noncoherent component is negligible, and the total power received by the antenna can be approximated by the coherent part only [5], which is given by

$$P_{\text{pol,coh}} = R_{\text{pol}} \frac{P_t G_t G_r \lambda^2}{(4\pi)^2 (r_1 + r_2)^2} \tag{1}$$

where the product $P_t G_t$ is the equivalent isotropic radiated power of the transmitted signal; G_r is the receiver antenna gain and λ is the wavelength ($\lambda =$ 19.042 cm for GPS L1 signal); r_1 and r_2 are, respectively, the distance between the receiver and the specular point and that between the specular point and the satellite; and

Manuscript received 28 December 2021.

Patrizia Savi and Yuekun Pei are with the Department of Electronics and Telecommunications, Politecnico di Torino, Corso Duca degli Abruzzi 24, 10129 Torino, Italy; e-mail: patrizia.savi@polito.it, yuekun.pei@polito.it.

Albert J. Milani is with Department of Mathematics, University of Wisconsin-Milwaukee, Milwaukee, WI 53211, USA; and the Dipartimento di Matematica, Università di Torino, Palazzo Campana, Via Carlo Alberto 10, 10123 Torino, Italy; e-mail: ajmilani@uwm.edu.

R_{pol} is the power reflectivity of the reflecting surface at a specified polarization. The reflectivity can be approximated by

$$R_{\text{pol}} = \left|\Gamma_{\text{pol}}\right|^2 \quad (2)$$

where Γ_{pol} is the Fresnel reflection coefficient. We consider the reflection at the boundary between air ($\varepsilon_{r1} = 1$) and a dispersive medium with complex relative permittivity (ε_{r2}). Then, in the case of normal (or horizontal, or TE) polarization n and parallel (or vertical, or TM) polarization p, the corresponding Fresnel reflection coefficients can be written, respectively, as

$$\gamma_n := |\Gamma_n| = \left|\frac{\cos\theta - \sqrt{\varepsilon - \sin^2\theta}}{\cos\theta + \sqrt{\varepsilon - \sin^2\theta}}\right| \quad (3)$$

$$\gamma_p := \left|\Gamma_p\right| = \left|\frac{\sqrt{\varepsilon - \sin^2\theta} - \varepsilon\cos\theta}{\sqrt{\varepsilon - \sin^2\theta} + \varepsilon\cos\theta}\right| \quad (4)$$

where $\varepsilon = \varepsilon_{r2}/\varepsilon_{r1}$. Our goal is to solve the inverse problem, consisting of determining ε explicitly as a function of θ, γ_n, and γ_p from the Fresnel reflection coefficients.

3. Complex Permittivity Solutions

We consider an incident plane wave in medium 1. Given the incident angle θ and the perpendicular and parallel coefficients $\gamma_n = |\Gamma_n|$ and $\gamma_p = \left|\Gamma_p\right|$, with $0 \leq \theta < \pi/2$ and $0 < \gamma_p < \gamma_n < 1$, the complex permittivity ε of medium 2 can be determined by solving (3) and (4), interpreted as a nonlinear algebraic system in the two unknowns $\Re(\varepsilon)$ and $\Im(\varepsilon)$.

The solution to the system (3) + (4), in the form $\varepsilon = x \mp jy$ ($j^2 = -1$; we recall that $\varepsilon = x + jy$ is a solution if and only if its conjugate $\bar{\varepsilon} = x - jy$ is also a solution), is given by

$$x := \Re(\varepsilon) = 2u^2 - 2b_n u\cos\theta + 1 \quad (5)$$

$$y := \Im(\varepsilon) = 2u|v| \quad (6)$$

where

$$\left(2c_{np}\cos\theta\right)u = \left(b_n - b_p\right)\cos(2\theta) \quad (7)$$

$$v^2 = -u^2 + 2b_n u\cos\theta - \cos^2\theta \quad (8)$$

and

$$c_{np} := \left(b_n^2 - 1\right)\cos^2\theta - \left(b_n b_p - 1\right) \quad (9)$$

$$b_n := \frac{1+\gamma_n^2}{1-\gamma_n^2}, \quad b_p := \frac{1+\gamma_p^2}{1-\gamma_p^2} \quad (10)$$

$$a_n := \frac{1+\gamma_n}{1-\gamma_n}, \quad a_p := \frac{1+\gamma_p}{1-\gamma_p} \quad (11)$$

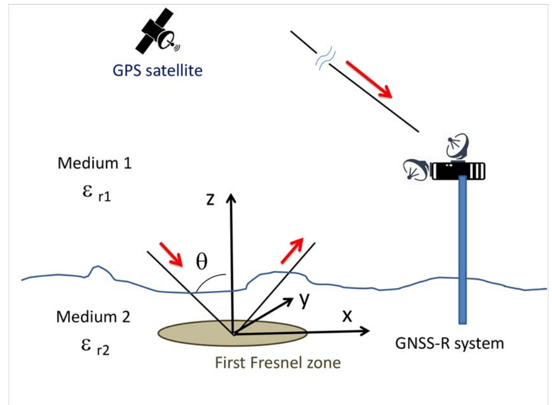

Figure 1. GNSS reflectometry geometry.

Note that $a_n > a_p > 1$, $b_n > b_p > 1$, $a_n > b_n$, and $a_p > b_p$.

The existence of a physically relevant solution—that is, with $\Re(\varepsilon) > 1$—requires that the right side of (8) be nonnegative (so that v, and hence y of (6), is defined), and that, in the right side of (5), $u > b_n\cos\theta$. In turn, these requirements translate into the double-inequality condition

$$b_n\cos\theta < u < a_n\cos\theta \quad (12)$$

which will be satisfied by the values of γ_n and γ_p measured at a given incidence angle θ (see Figure 2).

We further note that the right side of (8) is nonnegative also if

$$\frac{\cos\theta}{a_n} < u \leq b_n\cos\theta \quad (13)$$

but in this case $\Re(\varepsilon) \leq 1$, and the solution is not physically relevant.

3.1 Special Cases

The cases $\theta = 0, \pi/4, \pi/2$ require extra considerations.

When $\theta = 0$, (3) and (4) collapse into the single equation

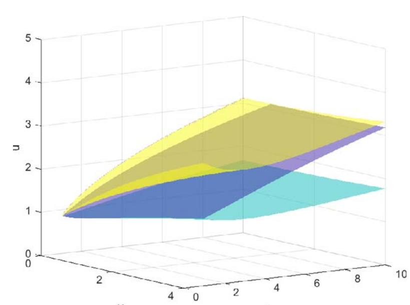

Figure 2. Case $\theta = \pi/6$. The blue surface is the range of u; the yellow and the green surfaces are, respectively, the upper and lower limits, as per (12).

$$\left|\frac{1-\sqrt{\varepsilon}}{1+\sqrt{\varepsilon}}\right| = \gamma_n = \gamma_p =: \gamma \tag{14}$$

thus it is no longer possible to determine ε uniquely. In fact, if $\gamma = 1$, any negative real number would be a solution to (14), which confirms that this case has no physical meaning. If instead $\gamma < 1$, (5)–(7) yield a physically relevant solution for all $u \in [b, a]$, where $b = (1+\gamma^2)/(1-\gamma^2)$ and $a = (1+\gamma)/(1-\gamma)$.

When $\theta = \pi/4$, we distinguish two cases. If $\gamma_n^2 = \gamma_p$, (3) and (4) reduce to the single equation

$$2\left|\varepsilon - \sqrt{2\varepsilon - 1}\right| = \left|1 - \sqrt{2\varepsilon - 1}\right|^2 \tag{15}$$

and again it is not possible to determine ε uniquely. In fact, in this case $c_{np} = 0$, so that both sides of (7) vanish, independently of u. As a consequence, any $u \in \left[b_n/\sqrt{2}, a_n/\sqrt{2}\right]$ yields a physically relevant solution. If instead $\gamma_n^2 \neq \gamma_p$, then $c_{np} \neq 0$; thus, from (7), $u = 0$, so that $y = 0$, and $\varepsilon = x = 1$.

In the limit case $\theta = \pi/2$, (3) and (4) reduce to

$$\left|\frac{-\sqrt{\varepsilon - 1}}{+\sqrt{\varepsilon - 1}}\right| = \gamma_n = \gamma_p \tag{16}$$

and thus $\gamma_n = \gamma_p = 1$ (again, this has no physical meaning), and a_n, a_p, b_n, and b_p are not defined. Still, any complex number $\varepsilon \neq 1$ is obviously a trivial solution to (16).

3.2 Real Case

In some cases (for example, for nondispersive media), the imaginary part of ε can be neglected, and ε can be assumed to be a real number [17,18]. In this case, ε can still be found from either of (3) or (4), as long as the angle θ and the coefficients γ_n and γ_p satisfy a mutual compatibility condition, which can be checked explicitly and ensures that the corresponding two solutions coincide. In [19], explicit equivalent formulas for $\Re(\varepsilon)$ were given, assuming that $\Im(\varepsilon) = 0$. This solution corresponds to the limit case $u = a_n \cos\theta$; indeed, in this case, $y = 0$ and

$$\varepsilon = x = 1 + \frac{4\gamma_n \cos^2\theta}{(1-\gamma_n)^2} \tag{17}$$

Thus ε is a real number, $\varepsilon > 1$, and ε coincides with the real solution ε_n found in [19]. (In the other limit case $u = b_n \cos\theta$ of (12), $\Re(\varepsilon) = 1$, as expected.)

3.3 Nondispersive and Dispersive Media

For nondispersive media, it is usual to consider, instead of (3) and (4), their versions without moduli—that is, with γ_n and γ_p replaced, respectively, by Γ_n and Γ_p, where $-1 < \Gamma_n$ and $\Gamma_p < 1$ (see, e.g., [20–22]). These versions of the equations are derived under the assumption that ε is a real number (that is, for nondispersive soils); in fact, the corresponding explicit solutions are real. In particular, the solution of the analogue of (3) is

$$\varepsilon = \varepsilon_n = 1 - \frac{4\Gamma_n \cos^2\theta}{(1+\Gamma_n)^2} \tag{18}$$

and $\varepsilon_n > 1$ if and only if $\Gamma_n < 0$. In this case, (18) coincides with the real solution (17) of (3) found in [19], because $\gamma_n = |\Gamma_n|$. Similarly, the analogue of (4) has two real algebraic solutions ε_{p1} and ε_{p2}, with $\varepsilon_{p1} < 1 < \varepsilon_{p2}$ if $\Gamma_p < 0$. More importantly, if, as should be expected on physical grounds, the two equations have a common solution ε_c, then necessarily

$$\varepsilon_c = \frac{(1-\Gamma_n)(1-\Gamma_p)}{(1+\Gamma_n)(1+\Gamma_p)} \tag{19}$$

In particular, the dependence of ε_c on θ is only through Γ_n and Γ_p. Requiring that ε_c be equal to either ε_n or ε_{p1}, ε_{p2} introduces additional compatibility restrictions on the values of θ, Γ_n, and Γ_p. Note also that $\varepsilon_c > 1$ if and only if $\Gamma_n < 0$; if $\Gamma_n = 0$, then $\varepsilon_c = 1$, in which case also $\Gamma_p = 0$. (We recall that if ε is real and positive and $\varepsilon \neq 1$, the Γ_p also vanishes at the so-called Brewster angle $\theta_B = \arctan(\sqrt{\varepsilon})$; this angle is not defined if ε is complex not real.)

4. Examples

The expressions (5) and (6) for the real and imaginary parts of ε were verified as inverse formulas of the Fresnel coefficient equations (3) and (4) with some tests. For example, for $\theta = \pi/6$ and $\varepsilon = 2 + j3$, (3) and (4) yield $\gamma_n = 0.4503$, and $\gamma_p = 0.3442$. If we use these values of θ, γ_n, and γ_p in (5) and (6), we obtain $x = 1.9946$ and $y = 2.9985$. In Figure 2 the value of the variable u and its lower and upper limits given in (12) are shown as a function of the real and imaginary parts of ε. As another example, for $\theta = \pi/3$ and $\varepsilon = 2 + j1.28$, (3) and (4) yield $\gamma_n = 0.4990$ and $\gamma_p = 0.0999$. If we use these values of θ, γ_n, and γ_p in (5) and (6), we obtain $x = 2.0794$ and $y = 1.2799$. Finally, for $\theta = \pi/4$, $\gamma_n = 0.5$, and $\gamma_p = 0.2$, so that $\gamma_n^2 > \gamma_p$, we find $y = 0$ and $\varepsilon = x = 1$, in accord with the discussion of Section 3.1.

5. Conclusions

In GNSS-R soil applications, it is important to determine the permittivity ε of the soil from the measured received coherent power. This requires solving the Fresnel coefficient equations (3) and (4) in terms of the complex permittivity ε. For soil moisture or sea salinity applications (dispersive media), the imaginary part of ε cannot be assumed to be negligible. In the literature, the real and the imaginary parts of ε are mostly found numerically; but, in fact, (3) and (4) can be explicitly solved. We determine complex solutions with $\Re(\varepsilon) > 1$, for all angles $\theta \in [0, \pi/2[$ and all measurements $\gamma_n, \gamma_p \in]0, 1[$, with $\gamma_p \leq \gamma_n$, which satisfy the admissibility condition (12) and can be explicitly verified.

6. References

1. S. Jin, E. Cardellach, and F. Xie, *GNSS Remote Sensing: Theory, Methods and Applications*, Dordrecht, the Netherlands, Springer, 2014.
2. V. U. Zavorotny and A. G. Voronovich, "Scattering of GPS Signals From the Ocean With Wind Remote Sensing Application," *IEEE Transactions on Geoscience and Remote Sensing*, **38**, 2, March 2000, pp. 951-964.
3. M. Wiehl and B. Legresy, "Potential of Reflected GNSS Signals for Ice Sheet Remote Sensing," *Progress in Electromagnetics Research*, **40**, 2003, pp. 177-205.
4. A. Alonso-Arroyo, V. U. Zavorotny, and A. Camps, "Sea Ice Detection Using U.K. TDS-1 GNSS-R Data," *IEEE Transactions on Geoscience and Remote Sensing*, **55**, 9, September 2017, pp. 4989-5001.
5. D. Masters, P. Axelrad, and S. Katzberg, "Initial Results of Land-Reflected GPS Bistatic Radar Measurements in SMEX02," *Remote Sensing of Environment*, **92**, 4, September 2004, pp. 507-520.
6. W. Ban, K. Yu, and X. Zhang, "GEO-Satellite-Based Reflectometry for Soil Moisture Estimation: Signal Modeling and Algorithm Development," *IEEE Transactions on Geoscience and Remote Sensing,* **56**, 3, March 2018, pp. 1829-1838.
7. N. Pierdicca, A. Mollfulleda, F. Costantini, L. Guerriero, L. Dente, et al., "Spaceborne GNSS Reflectometry Data for Land Applications: An Analysis of Techdemosat Data," IGARSS 2018—2018 IEEE International Geoscience and Remote Sensing Symposium, Valencia, Spain, July 22–27, 2018, pp. 33-43.
8. W. Li, A. Rius, F. Fabra, E. Cardellach, S. Ribó, et al., "Revisiting the GNSS-R Waveform Statistics and Its Impact on Altimetric Retrievals," *IEEE Transactions on Geoscience and Remote Sensing*, **56**, 5, May 2018, pp. 2854-2871.
9. J. Mashburn, P. Axelrad, S. T. Lowe, and K. M. Larson, "Global Ocean Altimetry With GNSS Reflections From TechDemoSat-1," *IEEE Transactions on Geoscience and Remote Sensing*, **56**, 7, July 2018, pp. 4088-4097.
10. E. Cardellach, J. Wickert, R. Baggen, J. Benito, A. Camps, et al., "GNSS Transpolar Earth Reflectometry exploriNg System (G-TERN): Mission Concept," *IEEE ACCESS*, **6**, March 2018, pp. 13980-14018.
11. S. J. Katzberg, O. Torres, M. S. Grant, and D. Masters, "Utilizing Calibrated GPS Reflected Signals to Estimate Soil Reflectivity and Dielectric Constant: Results From SMEX02," *Remote Sensing of Environment*, **100**, 1, January 2006, pp. 17-28.
12. Y. Pei, R. Notarpietro, P. Savi, M. Cucca, and F. Dovis, "A Fully Software Global Navigation Satellite System Reflectometry (GNSS-R) Receiver for Soil Monitoring," *International Journal of Remote Sensing*, **35**, 6, 2014, pp. 2378-2391.
13. J. Wang and T. J. Schmugge, "An Empirical Model for the Complex Dielectric Permittivity of Soils as a Function of Water Content," *IEEE Transactions on Geoscience and Remote Sensing*, **GE-18**, 4, October 1980, pp. 288-295.
14. M. T. Hallikainen, F. T. Ulaby, M. C. Dobson, M. A. El-rayes, and L.-K. Wu, "Microwave Dielectric Behavior of Wet Soil—Part 1: Empirical Models and Experimental Observations," *IEEE Transactions on Geoscience and Remote Sensing*, **GE-23**, 1, January 1985, pp. 25-34.
15. R. D. De Roo and F. T. Ulaby, "Bistatic Specular Scattering From Rough Dielectric Surfaces," *IEEE Transactions on Antennas and Propagation*, **42**, 2, February 1994, pp. 220-231.
16. N. Pierdicca, L. Guerriero, M. Brogioni, and A. Egido, "On the Coherent and Non Coherent Components of Bare and Vegetated Terrain Bistatic Scattering: Modelling the GNSS-R Signal Over Land," 2012 IEEE International Geoscience and Remote Sensing Symposium, Munich, Germany, July 22–27, 2012, pp. 3407-3410.
17. P. Savi and A. J. Milani, "Real-Valued Solutions to an Inverse Fresnel Problem in GNSS-R," IGARSS 2018—2018 IEEE International Geoscience and Remote Sensing Symposium, Valencia, Spain, July 22–27, 2018, pp. 3327-3330.
18. Y. Jia, P. Savi, D. Canone, and R. Notarpietro, "Estimation of Surface Characteristics Using GNSS LH-Reflected Signals: Land Versus Water," *IEEE Journal of Selected Topics in Applied Earth Observations and Remote Sensing*, **9**, 10, October 2016, pp. 4752-4758.
19. P. Savi, S. Bertoldo, and A. Milani, "Determining Real Permittivity From Fresnel Coefficients in GNSS-R," *Progress in Electromagnetic Research M*, **79**, 2019, pp. 159-166.
20. R. De Roo and C.-T. Tai, "Plane Wave Reflection and Refraction Involving a Finitely Conducting Medium," *IEEE Antennas and Propagation Magazine*, **45**, 5, October 2003, pp. 54-61.
21. I. M. Besieris, "Comment on the 'Corrected Fresnel Coefficients for Lossy Materials,'" *IEEE Antennas and Propagation Magazine*, **53**, 4, August 2011, pp. 161-164.
22. A. Egido, G. Ruffini, M. Caparrini, C. Martin, E. Farres, et al., "Soil Moisture Monitorization Using GNSS Reflected Signals," Proceedings of the 1st Colloquium Scientific and Fundamental Aspects of the Galileo Programme, Toulouse, France, May 13–14, 2007, pp. 1-7.